Test Mass Ring Dampers with Minimum Thermal Noise

S. Gras*, D.G. Blair and L. Ju

School of Physics, The University of Western Australia, Stirling Highway, Crawley, WA 6009, Australia

Abstract

Advanced laser interferometers gravitational wave detectors may need to substantially reduce the Q-factor of test mass normal modes to eliminate parametric instability. In this paper we investigate various ring damper configurations for two different laser beam geometries. We show that there is a well defined location near the mid point of a test mass where the thermal noise degradation from the ring damper is minimised. A Q-factor reduction by a factor of 5 can be obtained for at least 30% of the investigated normal modes at the cost of a 1% increase in thermal noise as seen by a 5 cm diameter incident laser beam. Ring dampers can be up to about 10 mm wide while maintaining minimum thermal noise effect contribution. Of the remaining modes, 30% are very weakly damped.

Key words: Interferometric gravitational wave detector; Thermal noise; Test masses; Inhomogeneous loss

PACS: 05.40.Jc; 04.80.Nn

1 Introduction

The long baseline gravitational wave detectors LIGO and VIRGO are operating at their design sensitivity [1] or are close from it [2]. However it is well known that an approximate 10-fold increase in sensitivity is required to be certain of detecting known sources at a reasonable rate. To achieve the required increased sensitivity it is proposed that the laser power in the optical cavities be increased roughly 100-fold. This very high power combined with the requirement of very low thermal noise introduces the risk of opto-acoustic parametric instability [3,4]. The parametric gain which must be less than unity to avoid instability, scales with both optical power and acoustic Q-factor. However it is now well understood that thermal noise is only directly linked to test mass Q-factor in the limit of homogeneous acoustic losses [5]. In the case of low loss test masses with localised sources of damping the thermal noise penalty can be low [6]. DeSalvo, Torrie and Gretarsson [7] suggested that there exist a ring position on the test mass wall where losses have a minimum contribution to the thermal noise. In preliminary work we have already assessed the noise contribution to test masses from localised losses at their circumference [8]. These studies led to the idea of using carefully designed ring dampers to degrade acoustic mode Q-factors without increasing thermal noise. In this paper we present a thermal noise analysis for possible ring dampers. Our goal is to design the parameters of a damping scheme that will achieve significant increase in the acoustic loss of test mass normal modes that are likely to couple to parametric instability processes, at minimal cost in thermal noise. We

* Corresponding author. Address: School of Physics, The University of Western Australia, Stirling Highway, Crawley,WA 6009, Australia
Email address: sgras@cyllene.uwa.edu.au (S. Gras).

Table 1

Model properties.

Material		Young's modulus $[GPa]$	Poisson ratio	Density $[g/cm^3]$	Structural loss
Sapphire	Al_2O_3	400	0.23	3.983	10^{-8}
Silica	SiO_2	70	0.17	2.200	10^{-8}

restrict our consideration to laser beams of Gaussian and mesa beam profile [9,10].

In section 2 we describe our model and the numerical methods used in this simulation. In section 3 we evaluate the thermal noise effect of various damping ring configurations while in section 4 we evaluate the achievable acoustic mode damping for 20 acoustic modes due to the lossy ring. In section 5 we summarise our results and determine the most optimal ring damper configuration.

2 Model

In this paper we use finite element modelling to analyse the effect of a ring damper on mirror thermal noise, and test its ability to suppress acoustic mode Q-factors. The analysis was carried out for both sapphire and fused silica materials. The thermal noise analysis was based on full size 3D models whereas for the modal analysis, we used planar symmetries to model one quarter of the test mass in the shape of a wedge. Symmetry constraints were applied to the nodes at the x-z and y-z planes which correspond to the flat sides of the wedge, for the purpose of reducing the computational time. However by using planar symmetries we were limited to those acoustic modes which possess such

symmetry properties. Due to the small thickness and localisation of the ring damper, we took special care to obtain adequate mesh density in modelling the surface of the test mass side wall. To do so, several types of elements were used such as: 10-node tetrahedral and 20-node brick structural elements with transitional pyramid elements at these elements interface. The highest concentration of elements was at the side wall which was meshed entirely with brick elements, whereas the centre of the model was meshed with tetrahedral elements with less dense meshing. The brick elements allowed us to simulate a wide range of ring damper widths. The limit on minimum width was set by the dimension of brick elements in the z-direction. We confirmed the validity of our results by comparing models with different mesh densities.

We modelled cylindrical test masses with thickness of 130 mm and radius of 157 mm. Material properties used for this simulation are shown in Table 1. In our analysis we considered two sources of loss: the structural loss related to the test mass substrate and the ring damper loss. We assumed that structural loss was frequency independent and equal to 10^{-8} for both materials although some experimental data indicates frequency dependence of the fused silica loss angle [11,13]. We also did not include surface losses from optical coatings. These two assumptions allowed us to simplify the simulations which were already very complex and computationally intensive. Since optical coatings are the main source of the thermal noise in a test mass, neglecting coating loss results in overestimated contribution of the ring damper to the increase of the thermal noise. In other words, our results are only valid for non-coated test masses. Thus, the results presented here sets the upper limit of a thermal noise change due to the strip. The effect of frequency dependent loss is considered separately in section 6.2.

We defined our ring damper as a $20\mu m$ thick strip with various widths and loss

angles. Additionally we assumed that the ring is a part of the model substrate. Thus it has exactly the same elastic properties as a substrate except for the loss which is a variable. With this ring definition the problem of contact elements is eliminated. We believe that this simplification is not inconsistent with practical designs as long as the ring is well acoustically impedance matched to the substrate. For example it could be created as a hard sputtered coating. Our results show that for rings less than 10 mm wide the loss contribution scales linearly with width. It also scales with volume and loss angle. Thus from our results rings can be defined by scaling the loss angle and ring volume. However we note that there are rather few hard materials with loss angles high enough to allow damping strips as thin as we assumed.

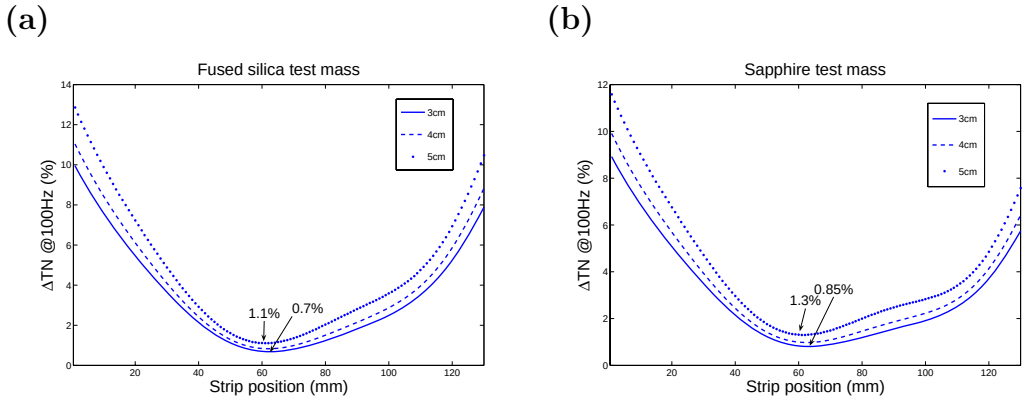

Fig. 1. Effect of a Gaussian laser beam size on thermal noise as a function of a strip position. In our simulation the laser beam is represent as a pressure profile applied on the front face of the test mass corresponding to x=130mm. The strip is $20\mu m$ thick, 1 mm wide with loss of 10^{-2}.

3 Thermal noise analysis

Thermal noise analysis was carried out for four different laser beam configurations. Test masses were made from either fused silica or sapphire. We considered Gaussian beams of 3,4 and 5 cm diameter and a mesa beam of diameter 10.4cm was also considered. The dissipation energy method [5] was adopted for this analysis. By this method the thermal noise spectral density $S(f)$ is determined by an integral over the volume dv of the test mass of a product of the strain energy $E(r)$ and the loss angle $\phi(r)$, normalised by a Boltzman factor and the laser beam profile. Thermal noise was estimated according to the following formula

$$S(f) = \frac{4k_B T}{\pi f} \int \frac{E(\vec{r})}{F_0(\vec{r})^2} \frac{\phi(\vec{r})}{\sqrt{\phi^2(\vec{r}) + 1}} dv, \tag{1}$$

where $F_0(\vec{r})$ is the transverse pressure profile corresponding to the laser beam profile produced by an oscillatory force integrated over the mirror face, k_B is Boltzmann's constant, f is frequency, and T is temperature. We do not make any assumtion about the small phase between strain and stress. Eqn.1 is a more general form of Levin's formula which allows us to estimate thermal noise for loss angle $\phi \leq 1$. A more detailed discussion of the mathematical formalism is given in Appendix 6.1.

Since it was essential to precisely estimate strain energy at the model side wall surface due to the applied pressure at the front face, we had to use inertia relief [12]. This technique balances the applied pressure by inertial forces induced by an acceleration field. We found that using any symmetry constrains on our test mass model causes inaccurate inertia relief calculation, which has direct impact on the surface energy estimation. Only the full model was free from

these undesired effects thereby ensuring that the strain energy was correctly estimated.

Our results show a clear thermal noise minimum position for the ring damper, but not exactly at the centre of the test mass side wall. We investigated how this thermal noise minimum position depends on laser beam size, ring position and width of the ring. Figure 1 shows how the Gaussian beam profile affects the thermal noise, for various locations of a 1 mm damping ring. The noise contribution reduces almost 10-fold when the ring is located at the 60 mm position, compared with one near a face. Each curve represents a different Gaussian beam spot size, 3, 4 and 5 cm, respectively. The y-axis corresponds to the percentage increase of the thermal noise due to the strip compared with the intrinsic modal thermal noise of the substrate read out by the same sized laser beam.

The effect of the strip width on the thermal noise is shown in Fig.2 and

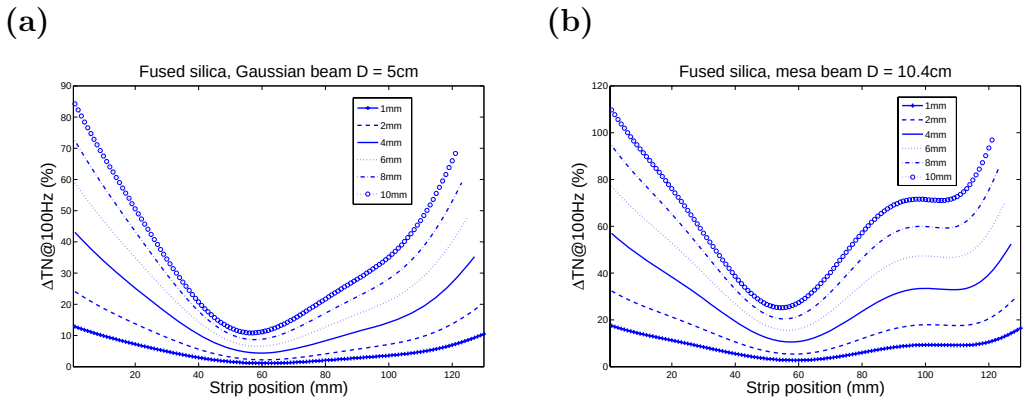

Fig. 2. Effect of the strip width on thermal noise as a function of a strip position for fused silica test masses. Both figures show thermal noise results for various strip widths as read out by (a) Gaussian laser beam with diameter of 5 cm and (b) Mesa laser beam with diameter of 10.4 cm, respectively. The ring is $20\mu m$ thick, with loss of 10^{-2}..The front face is at x = 130 mm.

Fig.3. We analysed 6 different strip widths assuming that the loss angle was 10^{-2}. Thermal noise was estimated for Gaussian beams with diameter of 5 cm and mesa beams with diameter of 10.4 cm. Figure 4 shows how thermal noise increases as the strip width increases, for all strips located at the optimal noise position. It is clear that mesa beam is more susceptible to the strip loss in comparison to the Gaussian beam. The linearity of the curves for small strip widths shows that for relatively narrow strips, there is no noise penalty in increasing the strip width such that $\phi \cdot Volume$ remains constant. This point is discussed further below.

4 Acoustic modes

We now go on to consider the damping of the normal modes for various damping ring configurations. The damping is represented in terms of quality factor variations. The quality factor Q is defined as follow

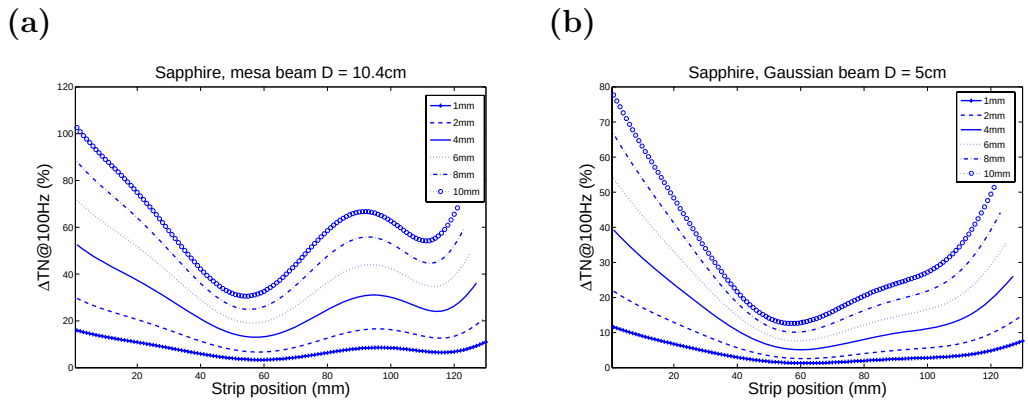

Fig. 3. Same as Fig.2 but for sapphire test masses.

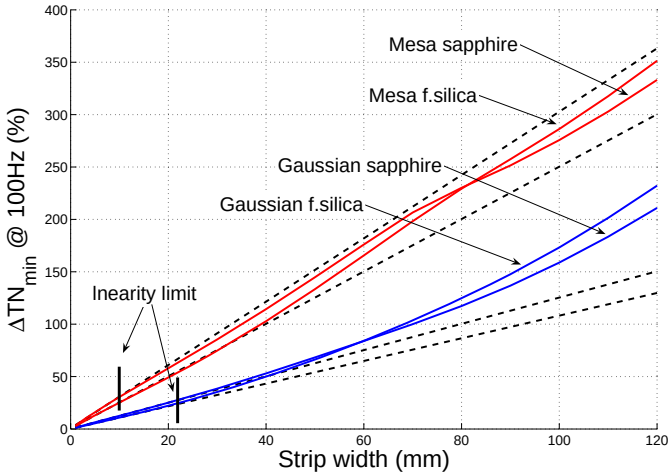

Fig. 4. Dependence of minimal thermal noise on strip width for fixed strip loss angle. ΔTN_{min} represents percentage degradation of a test mass modal thermal noise with the ring in respect to the modal thermal noise without the ring. Strip is defined in the same way like in the previous figures.

$$Q_n = \frac{\int E_n(\vec{r})dv}{\int E_n(\vec{r})[\frac{\phi(\vec{r})}{\sqrt{\phi^2(\vec{r})+1}}]dv}, \tag{2}$$

where E_n is the stored energy density for a given acoustic mode n, ϕ is the loss angle. The derivation of this formula is presented in Appendix 6.1.

Figure 5 shows damping of the first 10 acoustic modes for a sapphire test mass with a 1 mm ring at the position of minimal thermal noise. It is clear that some modes are poorly suppressed for such a strip configuration. Therefore we investigated the width and loss angle of the strip in more detail. To do this we set constraints on the minimum acceptable thermal noise amplification.

We analysed three different strip configurations for which thermal noise would increase by 1, 2 and 4%, respectively. Figure 6 shows the excess loss for the first 10 modes in a fused silica test mass, and the first 20 modes in a sapphire test mass. In each case we calculated the excess noise when a strip of 1 mm

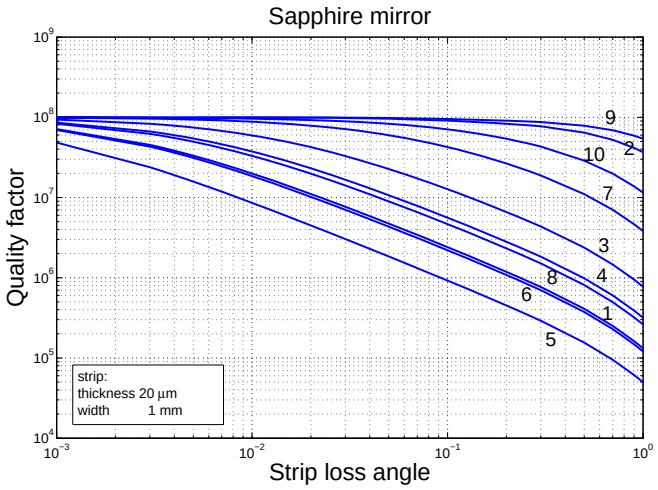

Fig. 5. En example of acoustic modes suppression due to a 1mm strip with various loss angles.

width has a loss contribution that causes 1%, 2% and 4% TN degradation of the thermal noise, respectively. In order to allow estimation for various combinations of the strip width and loss angle for the given thermal noise constraints, we produced maps of strip width versus loss angle as shown in Fig.7 and Fig.8. Each contour represents percentage thermal noise degradation estimated at the minimum positions. These maps allow us to choose losses for different strip widths.

The dependence of strip width on quality factor is shown in Fig. 9. Each line represents a mode excess loss as a function of a strip width with loss angle causing 1% thermal noise degradation. In this figure we can see 6 distinctive patterns of Q-factor reduction, marked with letters. The modes marked A have the greatest strain energy at the ring position while the modes E and F have weak coupling to the ring. Because some modes have similar shapes, their energy distributions are comparable. Figure 11 in the Appendix 6.3 shows the strain energy on the side walls. From that plot we can easily see that for some modes the ring damper may be very ineffective (Fig. 9 and Fig. 11F) whereas

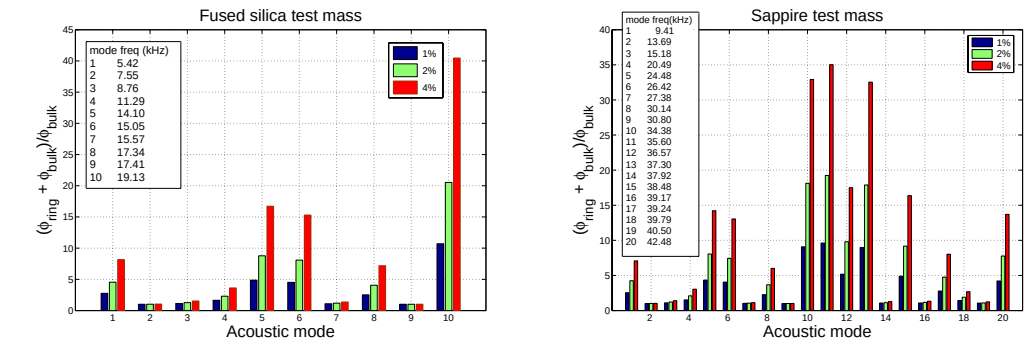

Fig. 6. Acoustic mode losses for different thermal noise constraints. A 1 mm strip is located at the optimal position where thermal nose reaches minimum. The loss angles used for sapphire were $7.3 \cdot 10^{-3}$, $1.5 \cdot 10^{-2}$ and $3.1 \cdot 10^{-2}$ corresponding to 1%, 2% and 4% TN degradation, respectively. For fused silica,the loss angles were chosen to be $9.0 \cdot 10^{-3}$, $1.8 \cdot 10^{-2}$ and $3.7 \cdot 10^{-2}$. The Y-axis represents an excess loss due to the strip. ϕ_{ring} and ϕ_{bulk} is the loss angle of the strip and the substrate, respectively.

other would be well damped (Fig.9 and Fig. 11A).

5 Discussion and Conclusion

Our numerical analysis reveals interesting aspects of ring damper design. First of all, the minimum thermal noise location is rather a shallow minimum, and there is no null point. Some curves show a point of inflection in the region 80 - 120 mm, and especially in sapphire with mesa beams this becomes secondary minimum. The shallowness of the minima means that damping rings may be wide without creating additional thermal noise as long as $\phi \cdot width$ remains constant. Our experience in modelling different thicknesses of damping rings leads us to believe that for rings located at the thermal noise minimum, with

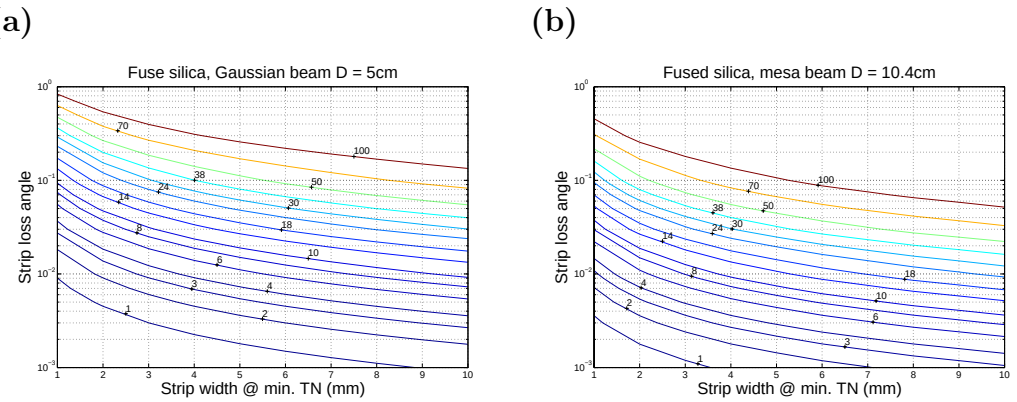

Fig. 7. Thermal noise map for a fused silica test mass model. Figure (a) and (b) corresponds to Gaussian and mesa laser beam profile, respectively. Each contour represents thermal noise amplification for a given strip configuration. For example, a 5 mm wide strip in Fig. 7a with loss angle of $2{\cdot}10^{-3}$ could increase test mass thermal noise by 1% with respect to the substrate thermal noise read out by Gaussian laser beam of 5cm.

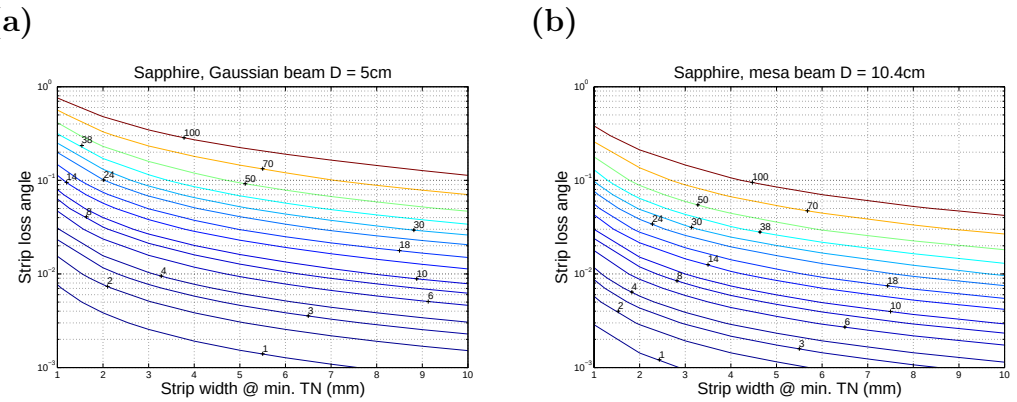

Fig. 8. Same as in Fig.7 but for the case of sapphire substrate.

width less than 10 mm, the thermal noise contribution and the Q-reduction scale directly as the product of $\phi \cdot ringvolume$. Thus our 20 μm ring thickness with $\phi \sim 10^{-2}$ could be replaced by a 2 mm thickness with $\phi \sim 10^{-4}$, as long as it is acoustically matched to the test mass. Our results show that small beam spots sizes appear to show lesser thermal noise degradation. While this

is true, we must remember that thermal noise increases inversely with spot size, so that there is no advantage in using smaller spots. The apparent disadvantage of mesa beams also disguises the intrinsically lower thermal noise of this configuration. The most important conclusion of this work is that the ring damper reduces the Q-factor of normal modes by varying degrees. A typical practical configuration can reduce the Q-factor of 30% of the normal modes by a factor of 5. To achieve one order of magnitude Q-reduction of more than

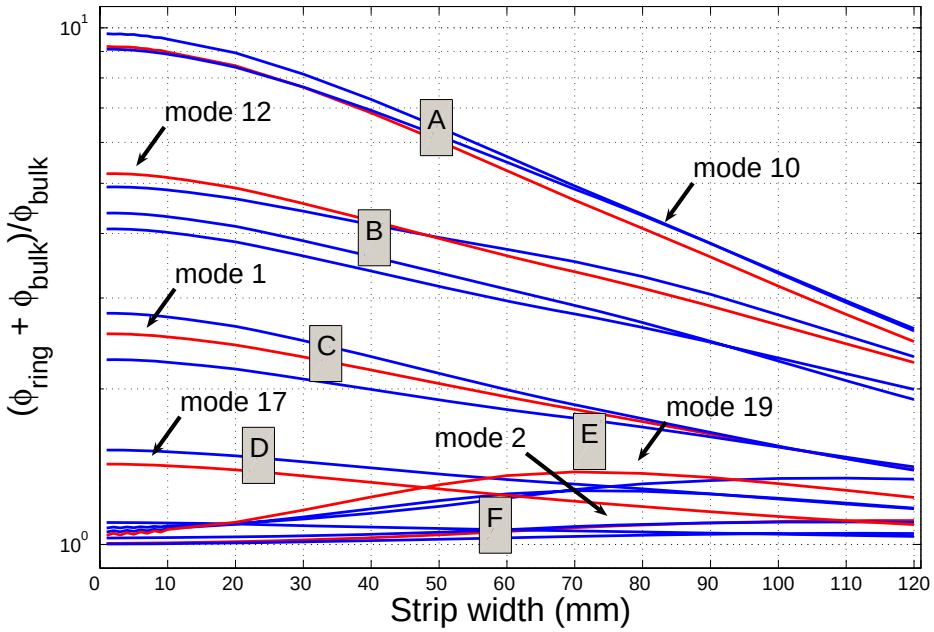

Fig. 9. Normal mode losses achievable by various strip configurations giving 1% thermal noise degradation. This plot represents 20 acoustic modes of the sapphire mirror. The loss angle was chosen in such way that for all strip widths the thermal noise increase was 1% compared with the bare substrate read out by a 5 cm Gaussian beam. The Y-axis has the same meaning as in Figure 6. The curves show that the narrowest strip gives the highest degradation, expect for mode groups E and F where degradation is small under all circumstances. The flatness of the modal curves between 0 and 10 mm again emphasise that strip width up to 10 mm scales as $\phi \times V_{ring}$.

half of the normal modes will have a thermal noise cost of $\sim 5\%$. Since Q-degradation was estimated with respect to the constant substrate loss, the results of our analysis provides information about the effectiveness of strip performance on the Q-value independent of the complications associated with surface losses. As detailed in Appendix 6.2, the frequency dependence of the loss angle in fused silica is responsible for additional decreasing of the Q-factor as the resonant frequency increases. This means that despite the Q-reduction due to the ring, there is an intrinsic factor which may cause additional degradation. For instance, the 10th resonant mode Q-factor should be 58% smaller than for assumed 10^8 value.

We recommend experimental studies of ring dampers using instruments such as the LIGO Thermal Noise Interferometer at Caltech. Effort will be required to identify suitable vacuum compatible, dense and hard damping materials that can be bonded to test masses. Optical coatings, if thick enough, could be useful candidates.

We have presented contour curves that allow the definition of damping ring parameters in terms of thermal noise degradation. This can be used to design possible damping rings. However, because the analysis depends on the test mass geometry, these curves are only strictly valid for the particular test mass geometry considered here. Moreover, optical coatings, which we do not consider here, have a significant impact on thermal noise. Such a loss source lowers the percentage degradation of the thermal noise due to the strip itself but also sets the higher thermal noise level due to this additional loss.

For the purpose of predicting parametric instability in advanced GW detectors it is necessary to know the quality factors of $\sim 10^3$ normal modes. Unfortunately the solution of equation 2 is extremely computationally intensive and the full solution including optical coatings is beyond our computa-

tional resources at the moment. In future work we expect to be able to obtain quantitive estimates of the reduction of parametric gain achievable using ring dampers.

Acknowledgements

The authors thank Riccardo DeSalvo for useful discussions, and the LIGO Laboratory for their hospitality. This work was supported by the Australian Research Council and the Department of Education, Science and Training. The work is a part of the Australian Consortium for Interferometric Gravitational Astronomy.

References

[1] LIGO http://www.ligo.caltech.edu/docs/G/G050509-00/G050509-00.pdf

[2] VIRGO http://www.ligo.caltech.edu/docs/G/G050510-00/G050510-00.pdf

[3] Braginsky V B, Strigin S E, Vyatchanin S P Phys. Lett. A 287 (2001) 331

[4] Braginsky V B, Strigin S E, Vyatchanin S P Phys. Lett. A 305 (2002) 111

[5] Levin Y, Phys. Rev. D 57 (1997) 659.

[6] Yamamoto K, Ando M, Kawabe K, Tsubono K Phys. Lett. A 305 (2002) 18

[7] DeSalvo R, "The challenge of Low Frequency G. W. Detection", http://www.ligo.caltech.edu/docs/G/G050521-00/G050521-00.pdf

[8] Gras S, Zhao C, Ju L, Blair D G J. Phys.: Conf. Ser. 32 (2006) 251

[9] Bondarescu M, Thorne K S, Phys. Rev. D (2004), ArXiv:gr-qc/0409083

[10] D'Ambrosio, Phys. Rev. D 67 (2003) 102004

[11] Numata K, Yamamoto K, Ishimoto H, Otsuka S, Kawabe K, Ando M, Tsubono K Phys. Lett. A 327 (2004) 263

[12] http://www.ansys.com

[13] Penn S D, Ageev A, Busby D, Harry G M, Gretarsson A M, Numata K, Willems P (2005) 2004; available at http://www.ligo.org/pdf-public/penn.pdf

6 Appendix

6.1 Derivation of the energy dissipation

Dissipation can be defined as

$$\Delta E =< \frac{dE}{dt} >=< F \cdot \dot{q} >, \tag{3}$$

where q is the displacement(or strain) due to the applied force(or stress). If the force(stress) is in the form of $F = F_0 sin(\omega t)$, than displacement(strain) may be written as $q = q_0 sin(\omega t - \sigma)$ where σ is the angle by which displacement lags behind the applied force(stress). The energy dissipation may now be written as

$$\Delta E =< F_0 \omega q_0 sin(\omega t) cos(\omega t - \sigma) >= \frac{1}{2} F_0 \omega_0 sin(\sigma), \tag{4}$$

Because the total strain energy in an acoustic mode (an analogy to the total energy of the spring) is $E_{mode} = \frac{1}{2} F_0 q_0$, therefore $\Delta E = \omega E_{max} sin(\sigma)$.
The definition of the loss angle in anelastic solid is

$$\phi(\omega) = \frac{ImY(\omega)}{ReY(\omega)}, \tag{5}$$

where Y is the Young modulus. Since the angle between $|Y|$ and $ReY(\omega)$ corresponds to the lag angle σ we can write $\phi = tan(\sigma)$. It is clear that if $\sigma \ll 1$ hence $\phi \simeq \sigma$ and $\Delta E = \omega E_{max} \phi$. This is the Levin result [5]. However for arbitrary σ we have

$$sin(\sigma) = sin(tan^{-1}(\phi)) = \frac{\phi}{\sqrt{\phi^2 + 1}}, \tag{6}$$

where $tan^{-1}(x) = sin^{-1}(\frac{x}{\sqrt{x^2+1}})$.

therefore

$$\Delta E = \omega E_{mode}(\frac{\phi}{\sqrt{\phi^2+1}}) \tag{7}$$

Substituting the energy dissipation in the Eqn.1 in Levin's paper [5] we obtain the displacement noise spectral density given by

$$S(f) = \frac{4k_BT}{\pi f}\int \frac{E(\vec{r})}{F_0(\vec{r})^2}\frac{\phi(\vec{r})}{\sqrt{\phi^2(\vec{r})+1}}dv, \tag{8}$$

which is a more general result than that of Levin. This is the equation used in section 3.

The quality factor is defined as

$$Q = 2\pi\frac{E_{mode}}{E_{cycle}} = 2\pi\frac{\int E_{mode}(\vec{r})dv}{\int E_{cycle}(\vec{r})dv)} \tag{9}$$

where E_{mode} is the total strain energy stored in a mode and E_{cycle} is the total energy dissipation per one cycle in a given mode. $E_{cycle} = (2\pi/\omega)\Delta E$ thus substituting E_{cycle} in above equation we get

$$Q = \frac{\int E_{mode}(\vec{r})dv}{\int E_{mode}(\vec{r})[\frac{\phi(\vec{r})}{\sqrt{\phi^2(\vec{r})+1}}]dv}. \tag{10}$$

6.2 Fused silica loss frequency dependence

Recently it has been reported that fused silica loss angle may be frequency dependent. Penn et al. [10] have shown that

$$\phi_{bulk} = a \cdot f^b, \tag{11}$$

where a, b are constants, and f is the frequency. According to the authors these constants vary dependent on the sample. For our consideration we adopt one of the suggested values of $7.15 \cdot 10^{-12}$ and 0.822 for a and b, respectively. Therefore the substrate loss angle value in Fig. 10 corresponds to the mode frequency in the range from 5 kHz up to few 100 kHz. Because we have studied

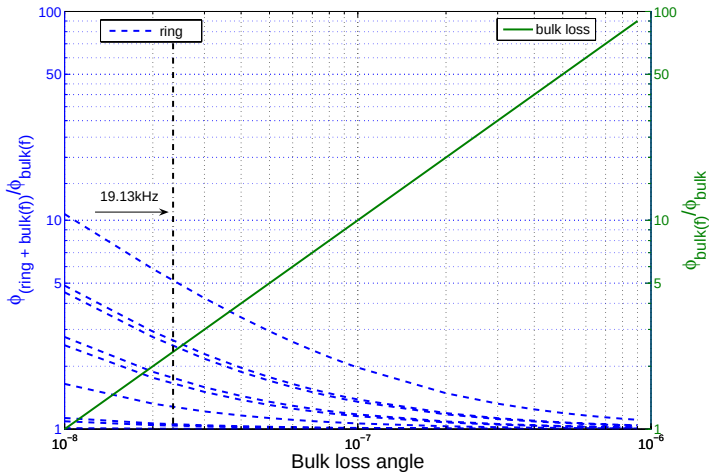

Fig. 10. Effect of bulk loss angle frequency dependence on Q-reduction. The right Y-axis represents the excess loss due to the strip whereas the left Y-axis corresponds to the excess loss due to the frequency dependence of the intrinsic loss. Each dashed line corresponds to the first 10 modes of the fused silica test mass. The solid line is the Q-degradation due to the frequency dependent intrinsic loss $\phi_{bulk(f)}$ with respect to the fixed intrinsic loss $\phi_{bulk} = 10^{-8}$ used throughout in this paper. The strip is 1 mm wide with a loss angle of $\phi_{ring} = 9.0 \cdot 10^{-3}$. The dashed vertical line shows the position of the 10th acoustic mode. The loss angle for this particular mode is 2.3 times bigger then the assumed value 10^{-8}. It is clear that for some modes it could be a dominant Q-reduction factor.

only modes in the small range from 5 kHz up to 20 kHz the bulk loss angle can be reduced at most by a factor of 2.3 in respect to assumed constant 10^{-8}value. Thus for the frequency dependent loss, the Q-factor can be in fact 0.6 orders

of magnitude smaller than our assumption. However according to Fig. 10 it can be seen that for high frequencies Q-reduction becomes less effective as the bulk loss increases for a given ring damper configuration. In the high frequency regime the bulk loss plays crucial role in the Q-reduction, as shown in Fig. 10.

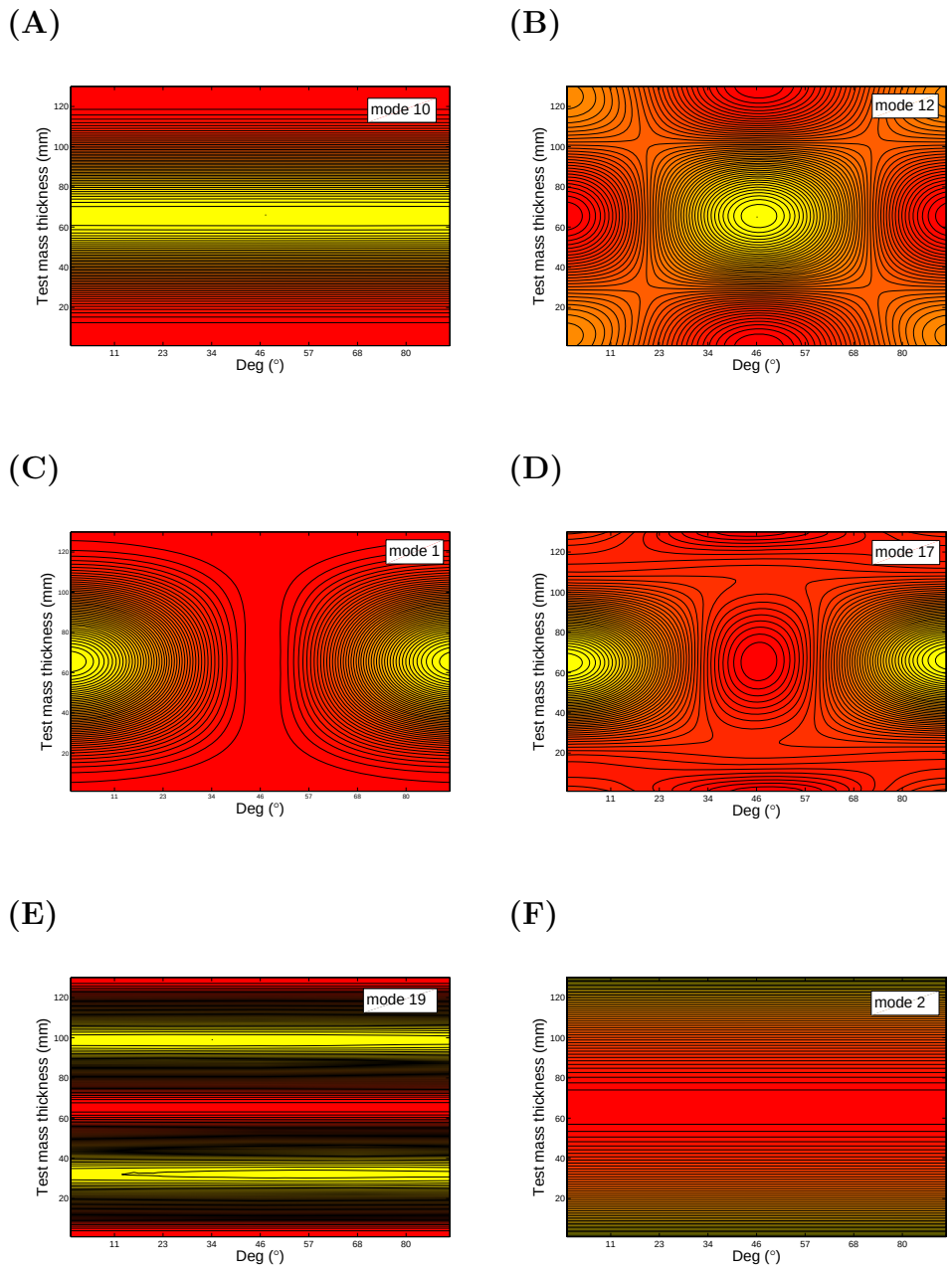

Fig. 11. Strain energy concentration in the side wall of test masses. Each plot corresponds to a different mode family shown in Figure 9. The intensity on the plots is related to the energy value, the lighter the spots the higher the energy at this position. The X-axis indicates the circumferential angle of a quadrant of the test mass.